

Locomotion of a flexible one-hinge swimmer in Stokes regime

Priyanka Choudhary

Department of Physics, Malaviya National Institute of Technology Jaipur, Jaipur, 302017 (India)
Department of Physics, Indian Institute of Technology Delhi, Hauz Khas, New Delhi 110016 (India)

Subhayan Mandal

Department of Physics, Malaviya National Institute of Technology Jaipur, Jaipur, 302017 (India)

Sujin B. Babu

Department of Physics, Indian Institute of Technology Delhi, Hauz Khas, New Delhi 110016 (India)
(Dated: June 14, 2022)

E. M. Purcell showed that a body has to perform non-reciprocal motion in order to propel itself in a highly viscous environment. The swimmer with one degree of freedom is bound to do reciprocal motion, whereby the center of mass of the swimmer will not be able to propel itself due to the Scallop theorem. In the present study, we are proposing a new artificial swimmer called the one hinge swimmer. Here we will show that flexibility plays a crucial role in the breakdown of Scallop theorem in the case of one-hinge swimmer or two-dimensional scallop at low Reynolds number. To model a one-hinge artificial swimmer, we use bead spring model for two arms joined by a hinge with bending potential for the arms in order to make them semi-flexible. The fluid is simulated using a particle based mesoscopic simulation method called the multi-particle collision dynamics with Anderson thermostat. Here we show that when our swimmer has rigid arms, the center of mass of the swimmer is not able to propel itself as expected from the Scallop theorem. When we introduce flexibility in the arms, the time reversal symmetry breaks in the case of the one-hinged swimmer without the presence of a head contrary to the one-armed super paramagnetic swimmer which required a passive head in order to swim. The reduced velocity of the swimmer is studied using a range of parameters like flexibility, beating frequency and the amplitude of the beat, where we obtain similar scaling as that of the one-armed super paramagnetic swimmer. We also calculate the dimensionless Sperm number for the swimmer and we get the maximum velocity when the Sperm number is around ~ 1.7

I. INTRODUCTION

Microorganisms have adapted their locomotion to the harsh environment of low Reynolds number regime by invoking different swimming strategy [1]. For example, the E. Coli moves with the help of helical wave passing through its flagellum [2, 3], Chlamydomonas flagella have a breast stroke kind of motion [4], African Trypanosome has a helical flagellum attached to the cell body with a planar wave passing through it [5, 6] etc. Swimming of these kind of natural swimmers have been investigated for the last half-century [1–9]. As a result of these studies, artificial swimmers have also been proposed, like Taylor sheet [10], Purcell’s two-hinge swimmer [11, 12], three-linked spheres swimmer [13] etc, which have further enhanced our understanding about low Reynolds number swimmers. One of the challenges in proposing an artificial swimmer lies in the fact that the proposed movement stroke should not be reciprocal otherwise it cannot propel itself due to the Scallop theorem. In Scallop theorem, Purcell had argued that a swimmer with one-hinge or one degree of freedom is bound to perform reciprocal motion and thus will not be able to swim in the Stokes regime [1, 11].

Purcell proposed two possible ways to elude from Scallop theorem, one is ”corkscrew” [2, 14] motion and second is ”flexible oar” [15, 16] motion. Using the concept of flexible oar, Dreyfus et al. [17] reported a micro swimmer that exploit elastic property of a slender filament made up of paramagnetic beads. To break the time inversion symmetry, a passive head was attached to the flexible arm. The passive head reduces the velocity of the flexible swimmer, bigger the head, higher is the drag force experienced by the swimmer. The head is essential for swimming because without it the tail performs a reciprocal motion and the velocity of the swimmer reduces to zero [18].

In the present study, we design and simulate a two-dimensional swimmer having two symmetric arms joined by a single hinge that looks like a two-dimensional scallop. The arms of the swimmer are semi-flexible and thus behave as an elastic scallop. To design an elastic scallop swimmer we use bead spring model [19] for the two arms joined by a common bead which acts as a hinge and to introduce flexibility to the two symmetric arms of the swimmer, we use bending potential [20]. The actuation happens only at the hinge and the rest of the arm relaxes depending on the strength of the actuation similar to the one-armed flexible swimmer [15]. In case of the elastic scallop the time inversion symmetry is broken because through the viscous drag term time enters into the equation of the filament shape, similar to the one-armed swimmer. Hydrodynamic interactions between the arms of the swimmer are implemented using the particles based simulation method for the fluid called as multi-particle collision dynamics (MPC) [21]. The advantage of MPC is that it solves the Navier-Stokes equation and also has inherent thermal fluctuations [22, 23] resembling real fluids. By this method a variety of hydrodynamic problems have been solved, for example, swimming of sperm cells [24], African Trypanosome [6], E. coli [25], Taylor line [26], Spheroidal microswimmer [27], Squirmer [28, 29] etc. This is the method of our choice as it is very easy to implement and is also shown to be one of the most efficient method in the Stokes limit [21].

We know that the dynamics of the one-armed swimmer is described by the non dimensional hyper diffusion equation given by Wiggins et al. [15, 30]. They have already shown that a flexible slender filament is propelled by periodic actuation, which is characterized by a dimensionless number called the Sperm number S_p [15]. Sperm number is the ratio of the length of the swimmer to its hydrodynamic penetration length. When $S_p \ll 1$, the penetration length is larger than the length of the swimmer, which means that the arms of the swimmer are stiff and perform near reciprocal motion, because of that we get very small velocity. When $S_p \gg 1$, we have the length of the swimmer to be very large compared to the penetration length, and hence the drag forces acting on the swimmer increase, thus the velocity of the swimmer again reduces. The interplay between these two effects leads to a maximum in the velocity at a point when the hydrodynamics penetration length is approximately equal to the length of the swimmer as shown by Wiggins et al. [15, 30].

The paper is arranged as follows. In section II we describe the model of our two-dimensional swimmer using bead spring and bending potentials. Then we briefly describe the particle based simulation technique MPC and also explain how we couple the swimmer with the solvent particles to properly resolve hydrodynamic interactions. In section III we discuss how our one-hinge swimmer breaks time inversion symmetry with flexible arms. We also study the velocity of the swimmer as a function of bending potential, frequency of actuation and amplitude of the actuating wave. We are able to define the dimensionless Sperm number for this swimmer and also discuss how our dimensionless velocity vary with respect to S_p . In section IV we discuss how this artificial swimmer can be realized experimentally, followed by the conclusions in section V.

II. COMPUTATIONAL METHODS

A. Multiparticle collision dynamics (MPC)

To simulate our artificial swimmer in two-dimensional Newtonian fluid, we make use of the coarse-grained simulation technique called multi-particle collision dynamics (MPC). Although there are different variation of MPC, we use the technique MPC with Anderson thermostat, where both linear and angular momentum are conserved [21]. We know that MPC solves the Navier-Stokes equation and has been shown to be computationally efficient method for low Reynolds number hydrodynamics [21]. MPC is a particle based method where we use fictitious point particles of mass m_0 to mimic the fluid. MPC consists of two steps, one is called the streaming step and another one is called the collision step. In streaming step, we update the position $\mathbf{r}_i(t)$ of all the solvent particles at time t according to

$$\mathbf{r}_i(t + \delta t) = \mathbf{r}_i(t) + \delta t \mathbf{v}_i(t). \quad (1)$$

Where $\mathbf{v}_i(t)$ is the velocity of i_{th} particle at time t and δt is the MPC time step.

The collision step is performed by dividing the simulation box into the square cells of unit length ($a_0 = 1$). In the present study, we keep the number of fluid particles per cell as 10, with periodic boundary conditions. The initial velocities of the particles are assigned from a Gaussian distribution with variance $k_B T / m_0 = 1$, where we consider unit mass of each fluid particle. In collision step, the velocity of each particle $\mathbf{v}_i(t)$ is updated according to

$$\mathbf{v}_i(t + \delta t) = \mathbf{u}(t) + \mathbf{v}_i^{ran} - \sum_{i \in cell} \mathbf{v}_i^{ran} / N_c + \left\{ m_0 \mathbf{I}^{-1} \sum_{j \in cell} [\mathbf{r}_{j,c} \times (\mathbf{v}_j - \mathbf{v}_j^{ran})] \times \mathbf{r}_{i,c} \right\}. \quad (2)$$

Where $\mathbf{u}(t)$ is the center of mass velocity of all particles in a cell, \mathbf{v}_i^{ran} is a random velocity taken from a Gaussian distribution with variance $k_B T / m_0 = 1$, N_c is the number of particles in a cell, \mathbf{I} is the moment of inertia of all the particles in a cell, $\mathbf{r}_{i,c} = \mathbf{r}_i - \mathbf{R}_c$ is the relative position of i_{th} particle in a cell with respect to the center of mass position \mathbf{R}_c of all the particles in a cell.

The swimmer keeps on actuating thereby pumping energy into the fluid which increases the kinetic energy of the fluid particles, and therefore the temperature of the fluid also increases known as viscous heating. The Anderson's thermostat which is inherent in the simulation technique, keeps the temperature of our system constant. In collision rule MPC conserves both linear as well as angular momentum. In MPC simulation, we know that when $\delta t \ll 1$, fluid particles become correlated thereby the system no longer remains Galilean invariant. In order to restore Galilean invariance we perform a random shift of the simulation box in the interval $[-a/2, a/2]$ as proposed by Ihle et al. [31, 32]. One of the advantage of MPC is that, we have analytical expressions for the calculation of transport coefficients [21]. The total kinematic viscosity ν is the sum of the kinetic viscosity ν^{kin} and collision viscosity ν^{col} , we always consider $\nu^{kin} = 0.61\delta t$ and $\nu^{col} = 0.036/\delta t$. In the present work we keep $\delta t = 0.01$, which keeps the kinematic viscosity $\nu \approx 3.6$ unless otherwise stated.

B. Modelling two-dimensional scallop

In order to model the two-dimensional swimmer with one-hinge, we consider a string of N odd numbered mass points connected with spring [19]. The middle bead acts as a hinge for the two-armed swimmer, so that the length of each arm is the same as shown in figure 1. The spring potential between the mass points is given by

$$U_s = \frac{1}{2} K_s (l - l_0)^2. \quad (3)$$

Where K_s is the spring constant, l is the distance between two mass points at any given time and l_0 is the equilibrium distance between the two mass points. In our simulation we keep the equilibrium spring length $l_0 = 0.5a_0$. To make sure that the springs remain relatively stiff during the simulations, we use a high spring constant $K_s = 10^8$ in the present study. The arms of the swimmer are made semi-flexible in nature by introducing a three body bending potential

$$U_b = K_b (1 - \cos \theta). \quad (4)$$

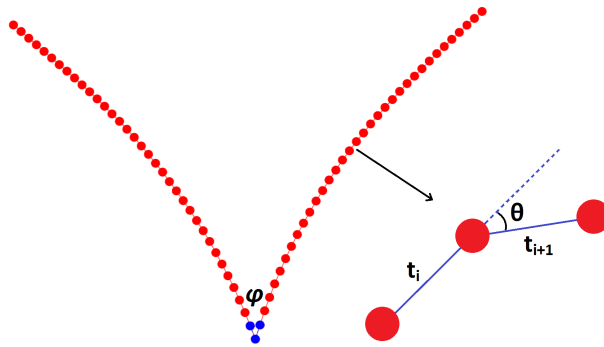


FIG. 1. The snapshot of a model one-hinge artificial swimmer with flexible arms. Three mass points are given blue color to show that the bending waves pass through only these three points. We have magnified the bond vectors t_i and t_{i+1} , which connect neighboring mass points and make an angle θ . φ is the angle between two arms near the hinge.

Where K_b is the stiffness constant, θ is an angle between two bond vectors \mathbf{t}_i and \mathbf{t}_{i+1} , as illustrated in figure 1 (magnified bond vectors) [19]. We apply the bending potential along both the arms of the swimmer except for the hinge points. When $K_b \rightarrow \infty$, we have rigid arms for the swimmer and for $K_b \rightarrow 0$, we have completely flexible arms. We vary the value of K_b from 10^4 to 10^7 , thereby vary the rigidity along the arms of the swimmer.

In order to simulate a two-dimensional scallop we define an angle φ (see figure 1) between the two arms of the swimmer, which oscillates between a minimum and maximum angle. In order to achieve this, we introduce a three body bending wave potential along the three blue colored beads given by

$$U_w = \frac{1}{2} K_w [t_{i+1} - \mathbf{R}(l_0 \alpha) t_i]^2. \quad (5)$$

Where K_w is a bending stiffness constant that decides the strength of the potential, \mathbf{R} is the rotation matrix, $\phi = l_0 \alpha$, $\alpha = A \sin^2(2\pi \nu t)$ is the spontaneous curvature between the mass points where the bending wave potential is applied, A is the amplitude of the wave and ν is the frequency with which the potential makes the beads to beat [6]. The matrix \mathbf{R} rotates one bond vector \mathbf{t}_i , against the neighboring bond vector \mathbf{t}_{i+1} , about a unit vector which is perpendicular to \mathbf{t}_i and \mathbf{t}_{i+1} , by an angle ϕ . As the curvature α is function of square of the sine wave, we will have only positive values for curvature, thus the angle φ between the arms can vary only between $0 - \pi$. When two arms are completely opened (i.e. zero curvature position), the angle φ will be the maximum $\varphi_{max} = \pi$ at that time, the value of $K_w = 4 \times 10^5$ is used in the present work. The total force on the i_{th} bead of the swimmer, due to spring and bending potentials is given by $\mathbf{F}_i = -\nabla_i(U_s + U_b + U_w)$. The movement of the swimmer is implemented by molecular dynamics (MD) technique. We update the velocities and positions of the beads using a leap frog velocity Verlet algorithm [20], where the integration time step is always kept at $\delta t_{MD} = 10^{-4}$.

C. Incorporation of swimmer with fluid particles

We perform n number of MD steps, where $n = \delta t / \delta t_{MD}$ before a MPC step. In streaming step of MPC, we only consider the fluid particles, and during this step we allow the fluid particle to pass through the swimmer as well. We in-cooperate the mass points of the swimmer with the fluid particles in the collision step, which give the correct hydrodynamics for the swimmer as already demonstrated by Babu et al. [19] for the case of semi-flexible sheets.

III. RESULTS

A. Breakdown of the time inversion symmetry

From the Scallop theorem, we know that the movement undergoing time reversal symmetry will not be able to propel in a low Reynolds number fluid. In the present work we simulate a two-dimensional one-hinge swimmer similar to a two-dimensional scallop. Figure 2(a) shows the shape conformation when we have flexible arms and figure 2(b) is when we have the rigid arms, for one complete cycle. During one complete cycle the curvature of the hinge undergoes

a change as $\sin^2(2\pi\nu t)$, which means we have only positive cycles. In figure 2(a) when we look from right to left, first half of the figure, (till the solid black line), $\sin^2(2\pi\nu t)$ changes from 0 to 1, shows the closing of the arms and the second half shows the opening of the arms with $\sin^2(2\pi\nu t)$ changing from 1 to 0. The curvature of the hinge changes as a function of the time ($\alpha = A \sin^2(2\pi\nu t)$) as given in the equation 5. When $t = 0$ we have zero curvature that means arms of the swimmer is opened to the maximum possible extent or we start from a straight line. As time progresses, α increases and the arms of the swimmer start to close from the center of the swimmer, similar to a two-dimensional scallop. When the arms start to close, the center of mass of the swimmer moves in the backward direction. The rest of the arms follow the actuation of the hinge points. As the actuation only happens on the hinge, there will be a delay for the actuation to reach the end of the arms. This will cause the points close to the hinge of the swimmer to close faster compare to the points further away. So as the arms close, the ends bend in an outward direction and resembles **V** shaped conformation. When it reaches $\sin^2(2\pi\nu t) = 1$, we get a maximum value of curvature equal to the amplitude A . After that the curvature at the hinge starts decreasing and the arms of the swimmer start to open up. Again the point away from the hinge will be moving in the closing direction, due to the delay in the propagation of the actuation. By that time the points close to the hinge would have already started to move in the opening direction. Due to this the ends of the swimmer are now bend inward as can be observed in the latter half of the figure 2(a). The center of mass of the swimmer also starts moving in the forward direction and the ends of the arms start to retract now in a **U** shaped conformation. At a later time, when the arms reach $\sin^2(2\pi\nu t) = 0$ or $\alpha = 0$, the arms of the swimmer are opened at maximum possible extent. As the swimmer has a **V** shape conformation during closing of the arms while in case of opening it has a **U** shaped conformation, thus breaking the time inversion symmetry and the one-hinge swimmer move ballistically from right to left as shown by the black arrow in figure 2, which was also predicted by E. Lauga [18]. The propulsion of the one-hinged swimmer is illustrated in the supplementary materials movie1. When we keep the bending stiffness $K_b = 10^7$, in our simulation we obtain rigid arms for one-hinge swimmer. In the case of rigid arms, the oscillations at the hinge are followed by every point of the arms and thus the swimmer performs reciprocal motion. There is no difference in the opening and closing conformation, as can be observed in figure 2(b). As a consequence the center of the mass of the swimmer does not undergo ballistic motion, as illustrated in the supplementary material movie2.

B. Mean squared displacement

To quantify the above observation we have calculated the mean square displacement of the center of mass for both flexible and rigid arm swimmer.

$$\langle \mathbf{R}^2 \rangle = \langle (\mathbf{r}_{cm}(t) - \mathbf{r}_{cm}(t_0))^2 \rangle. \quad (6)$$

Where $\mathbf{r}_{cm}(t_0)$ and $\mathbf{r}_{cm}(t)$ are the position of the center of mass of the swimmer at beginning of the simulation $t = 0$ and at time t respectively. In figure 3, we can see that in both the cases, till $t \approx 10$ swimmer does hardly move, because bending waves take some time to propagate from hinge to the end of the arms. As we have discussed in the previous section, initially a swimmer has open arms and with time it starts to close the arms due to that center of the mass displaces, we get an upswing in MSD. Once the curvature reaches the maximum, arms starts to open again and center of the mass tries to come back to the previous position and due to that we get a down swing in MSD. Here we consider the beating frequency $\nu = 0.01$, so at $t = 100$, a swimmer completes a cycle of oscillation by closing and opening the arms. Because of the oscillatory stroke that the swimmer performs, MSD of the swimmer always oscillates. After 3 – 4 cycles of oscillation the flexible swimmer starts to undergo ballistic motion characterized by the slope of 2, with the swimmer moving toward the left as indicated by the arrow in the figure 2(a), as predicted by E. Lauga [18]. For the rigid arms the center of mass of the swimmer undergoes diffusive motion characterized by $\langle \mathbf{R}^2 \rangle \propto t$ with a slightly enhanced diffusion coefficient ($D = \langle \mathbf{R}^2 \rangle / (4t) \approx 0.009$) due to the actuation of the arms. While the passive swimmer diffuses with a diffusion coefficient $D \approx 0.005$.

C. Effect of Flexibility

From the previous section we know in the present work flexibility plays a major role in the swimming of the two arms swimmer. To study the effect of flexibility we measure the reduced velocity after the swimmer has attained ballistic motion which is defined as $V_{cm}/L\nu$ where $V_{cm} = \sqrt{\langle R^2 \rangle}/t$ and L is the length of the arms of the swimmer. In figure 4, we plot the reduced velocity as a function of bending rigidity K_b of the arms of the swimmer. When $K_b = 0$ and $K_w = 0$ our swimmer becomes passive and behaves as a Gaussian polymer chain. When we increase K_b from 10^4 onward, keeping $K_w = 4 \times 10^5$, we observe a nominal increment in speed. The reason being that the arms of

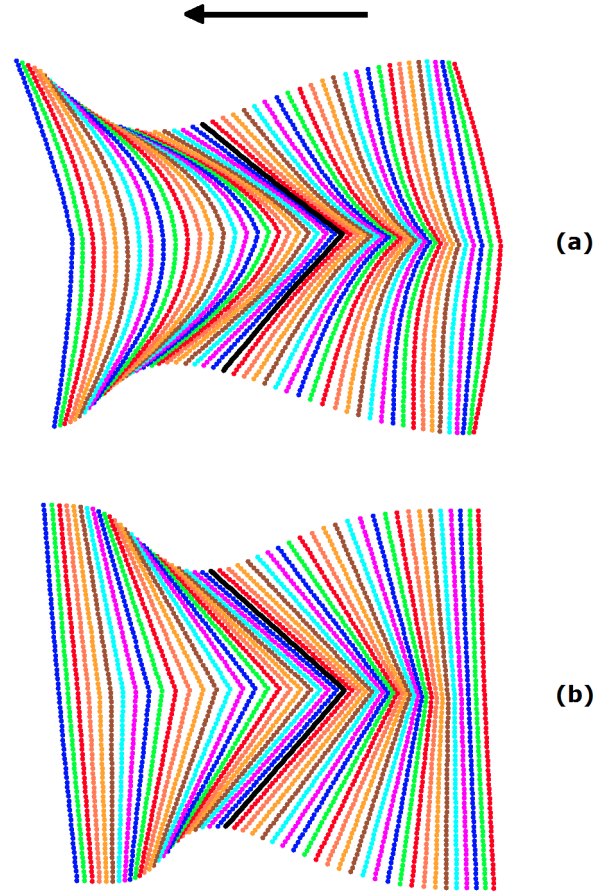


FIG. 2. Sequence of conformation of the arms (here different colors are used just for the better visualization) of the one-hinged swimmer over one complete beat cycle, (a) represents the case for a flexible arms and (b) for the case of rigid arms. From right to left, we observe the sequence of closing, from the center bold conformation shows the opening of the arms of the swimmer. The black arrow at the top shows the direction of swimming for the flexible swimmer.

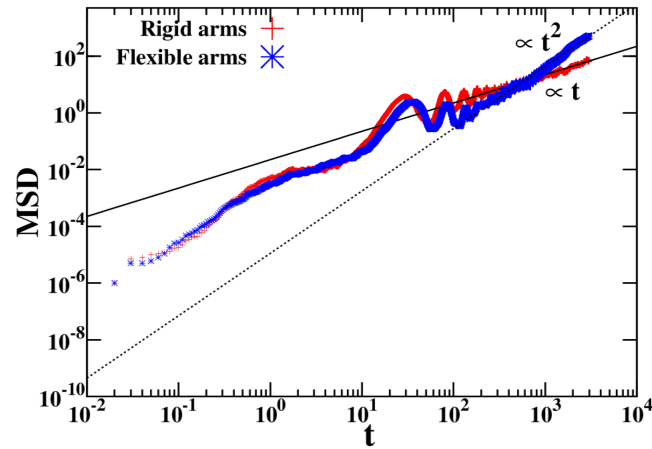


FIG. 3. Mean squared displacement of the center of mass position of the swimmer is plotted as a function of time t for the flexible arms (blue) and rigid arms (red). The solid line has slope of 1 indicating diffusive motion and dotted line has slope of 2 representing directed motion of the swimmer.

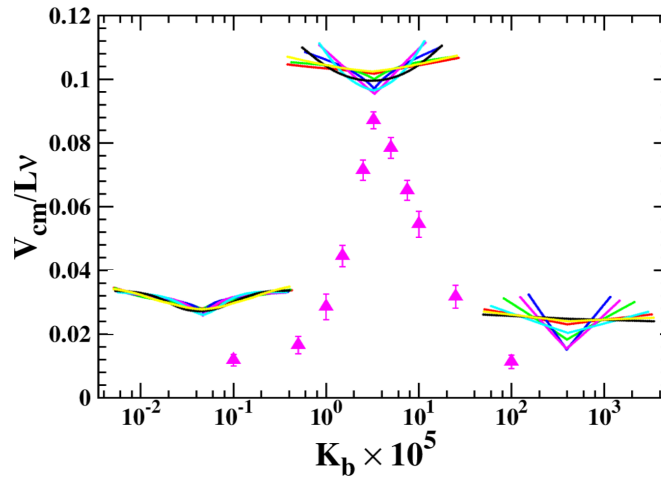


FIG. 4. The reduced velocity of the swimmer is plotted as a function of bending rigidity of the arms of the swimmer. We have also shown the typical shape conformations for three different K_b values, see text.

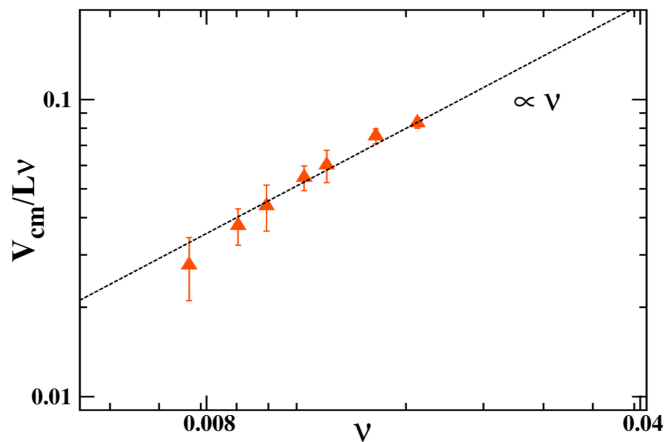


FIG. 5. The reduced velocity is plotted as a function of frequency of the actuation. The solid line has slope of one as predicted for the small amplitude approximation.

the swimmer are very flexible and the wave which passes from the hinge is damped before reaching the end point as shown in conformation portray for $K_b = 10^4$ in figure 4. We can observe here, that the configurations of the swimmer do not change appreciably during the entire beat cycle. The arms of the swimmer become progressively rigid by increasing K_b , the speed increases as shown in figure 4. Here we have a competition between the elastic forces of the swimmer and viscous drag because of the fluid particles. The speed starts to increase till it reaches a maximum when the elastic forces cancel the frictional forces, as shown in the typical shape configuration for intermediate bending stiffness $K_b = 3.25 \times 10^5$. On further increasing the rigidity of the arms, the change in shape conformation reduces and the swimmer undergoes the reciprocal motion, as can be observed in shape conformation profile for $K_b = 10^7$. Thus, it behaves as a conventional scallop and eventually the speed of the scallop goes towards zero as we keep on increasing the rigidity of the arms.

D. Beating frequency

In figure 5, we have plotted the reduced velocity of the swimmer with respect to the beating frequency ν imparted on the hinge. In the present study for the one hinge swimmer, we are considering only large amplitudes, the reduced velocity scales linearly with ν , as shown by the straight dashed line in the figure 5 which has slope of 1. For a single-armed swimmer Wiggins et al. had derived the equation for velocity using small amplitude approximation, where it was shown that the reduced velocity scales linearly with ν . In our case, the amplitude we have considered $A = 4.25$

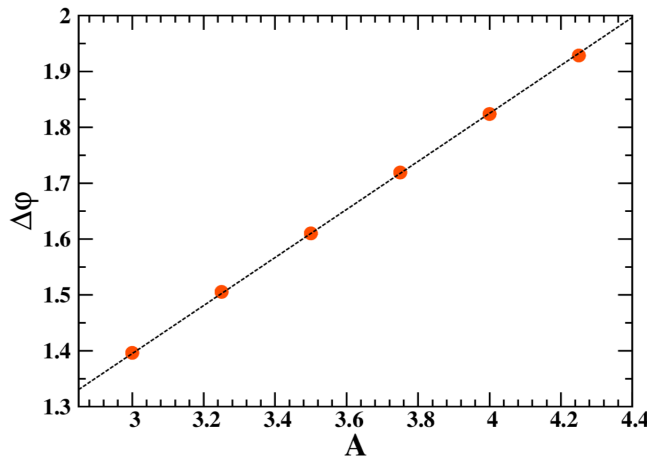


FIG. 6. $\Delta\varphi$ (in radian) is plotted as a function of the amplitude of actuation. The dashed line shows the linear fit given by $(0.43A + 0.1)$.

is large, still we observe that the scaling is in agreement with that of Wiggins et al. [15]. In the present study, we did not consider large values of frequency because it is well known that the MPC fluid is no longer incompressible for large ν , thereby we do not have the correct hydrodynamic interactions in the system [33].

E. Amplitude of the actuation

For closing and opening of the arms of the swimmer, the parameter that we are changing is the amplitude A of the bending wave given in the equation 5. The amplitude is chosen in such a way whereby we make sure that the mass points of the swimmer close to the hinge will never overlap. As we change the amplitude of the beating, the angle created between the arms φ of the swimmer changes as well, see figure 1. The maximum angle between the arms in the simulation nearly stays around $\varphi_{max} = \pi$, while the minimum angle varies between $\varphi_{min} = \pi/3 - 2\pi/3$. In the present study the amplitude is related to the difference in the minimum and maximum angle made by the arms of the swimmer. In figure 6, we plot the amplitude A as a function of $\Delta\varphi = \varphi_{max} - \varphi_{min}$, which is the difference between the minimum and maximum angle during the opening and closing of the arms of the swimmer.

When $\Delta\varphi = \pi$, then the maximum angle will be π and the minimum angle will be 0 between the arms of the swimmer, which means the arms of the swimmer is going to overlap at the minimum angle. For measuring φ , we calculate a unit vector between the hinge and the fourth bead from the hinge for the left arm \hat{p}_l and the right arms \hat{p}_r respectively. Then the angle $\varphi = \cos^{-1}(\hat{p}_l \cdot \hat{p}_r)$, also note that for the beating of the arms we are changing the spontaneous curvature of the beads close to the hinge by $\sin^2(2\pi\nu t)$, which means the angle between the arms will not go beyond π . The dashed line in figure 6 is drawn from straight line equation which shows that $A \propto \Delta\varphi$. In the present work we have kept $K_w \approx 10^5$, the we observe that arms can open and close in such a way $\Delta\varphi > \pi/3$.

In figure 7, we plot the reduced velocity as a function of the $\Delta\varphi$. Here we observe that as the difference in the angle between the arms increases the speed of the swimmer also increases. We observe that the reduced velocity scales as the square of $\Delta\varphi$, the dashed line in the inset of figure 7 has slope of two. The equation for the velocity has been deduced from the small amplitude approximation for the single-armed swimmer [15] as well as for the one-hinge swimmer [18]. In these works they had shown that the reduced velocity scales with the square of the amplitude of the actuation. Even though our amplitudes are larger than that were considered in these work, we observe that the reduced velocities have similar kind of scaling as that of small amplitude approximation. We were not able to further increase the amplitude of the actuation as that will lead to the overlap of the arms of the swimmer, which is not a physical scenario for an artificial swimmer.

F. Sperm number

Wiggins et al. had shown that if a flexible rod is perturbed at one end by $y_0 \cos \omega t$, for small amplitudes, the dynamics of the one arm follows the dimensionless hyper diffusion equation $\frac{dy}{dt} = S_p^4 \frac{d^4 y}{dx^4}$, where S_p is a dimensionless

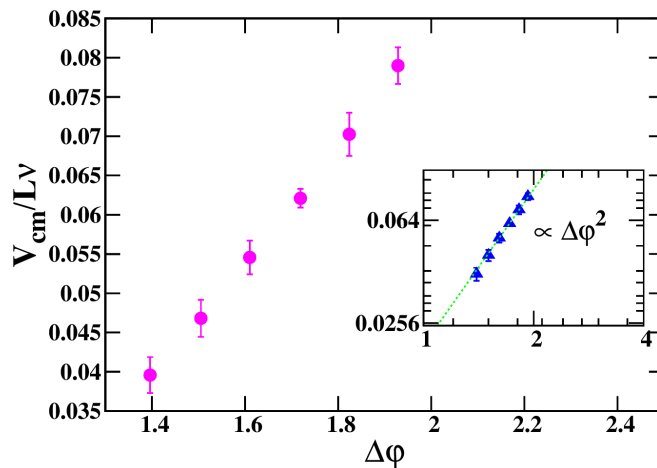


FIG. 7. Reduced velocity of the swimmer is plotted as a function of $\Delta\varphi$ (in radian), the dashed line (inset) has slope of two as predicted for small amplitude approximation.

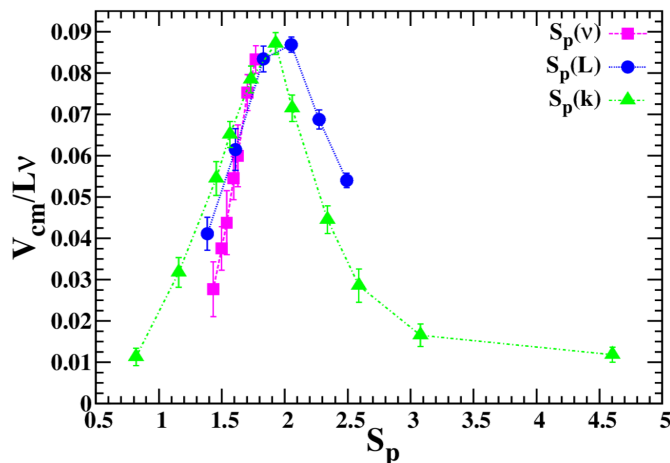


FIG. 8. The reduced velocity of the swimmer is plotted as a function of Sperm number. The value of S_p was varied, changing ν (square), L (circle) and k (triangle) keeping all other parameters the same.

number called Sperm number. The Sperm number is given by

$$S_p = L \left(\frac{\xi_{\perp} 2\pi\nu}{k} \right)^{\frac{1}{4}}. \quad (7)$$

Where L is the length of the arms of the swimmer, $k = K_b l_0$ is stiffness of the arms of the swimmer, ν is the frequency and ξ_{\perp} is the frictional coefficient per unit length in perpendicular direction of motion defined to be consistent with the one-armed swimmer. In the present study, we calculate the perpendicular friction coefficient using $\xi_{\perp} = 4\pi\eta/[\ln(L/r) + 1/2]$ [34], where η is the viscosity of the fluid and r is the radius of the arm. Since we have point particles which will not overlap, we have considered a very small value for $r = 0.01$. In figure 8 we show the reduced velocity of the swimmer as a function of the Sperm number. For the small value of the S_p we observe that the elastic forces dominate and we get a small velocity, while in the high Sperm number region the drag forces acting on the arms of the swimmer dominate and again the velocity goes down. As there is a competition between the viscous and elastic forces in the arms of the swimmer, there should be one particular S_p value where we should observe a maximum for the velocity, which is around ~ 1.7 in our case. For the one-armed swimmer with small amplitude approximation, it was shown that the maximum velocity is when $S_p \approx 4$, while Lagomarsino et al. have demonstrated using simulations that for the same one-armed swimmer with large amplitude, the maximum velocity happens when $S_p \approx 2$ [16, 35]. This is similar to our present work, where we consider the amplitude larger than the small amplitude approximation. In figure 8, S_p is varied by changing the length of the arms, the frequency of actuation and the stiffness K_b of the

arms of the swimmer keeping the rest of the parameter constant of the equation 7. Here we can see that the peak positions of the reduced velocities remain almost same. For the small values of the Sperm number till $S_p < 1.6$, we find continuous increment in scaled velocity with S_p as expected. After the maximum, we observe that the scaled velocity continuously decreases as we increase the S_p and after $S_p > 3$ we observe a slow and steady drop in scaled velocity. For small amplitude approximation Wiggins et al. had shown that the scaled velocity attains a plateau for higher S_p value. Our results are similar to the results obtained by Lagomarsino et al. [16], where they showed that for large values of S_p , when large amplitudes are considered, the velocity does not stay constant, it slowly decreases with S_p .

IV. DISCUSSIONS

It was shown that the one-armed flexible swimmer [17, 36] will undergo ballistic motion only if a passive head is attached to the arm. The two-armed swimmer with a head was initially considered by Lauga [18], for simplicity of the calculation he ignored the hydrodynamic interactions between the arms of the swimmer and also the velocity of the swimmer was derived under the infinitely small amplitude approximation. Lauga has also shown analytically that if two arms are actuated similar to a one-armed swimmer a passive head is not required to break the time inversion symmetry. In the present work we are able to show that if two filaments are joined by a hinge and actuated only at the hinge the artificial swimmer starts to behave as a self propelled object. We obtain the direction of the swimmer as predicted by Lauga [18] but the magnitude of velocity is not in agreement with our work. This may be because in the present work there are hydrodynamic interactions between the arms of the swimmer as well as the amplitude of the actuation in the present work is higher than that considered for the small amplitude approximation. Also recently Tian Quie et al. [37] demonstrated that a micro scallop can swim in a non Newtonian fluid. In this work they have used a rigid arm scallop in a non Newtonian fluid while in the present work our scallop or one-hinge swimmer have flexible arms thereby performing the ballistic motion even in Newtonian fluid. It is known that swimmer African Trypanosome velocity is increased approximately 8 times when it swims in a fluid (non Newtonian) having obstacles of size and spacing of RBC in blood [38] and it will be interesting to study the swimming of the one hinge swimmer in these environments.

Recently Haug et al. have shown that they can create soft robotic materials using light actuated materials [39]. The light-driven liquid-crystal (LDLC) material [40], which are sensitive to ultra-violet light, can convert light into the mechanical energy with quick response and large deformation. When we shine UV light the LDLC undergoes a phase transition by which it gets converted into a shorter molecule, while shining visible light it recovers its original conformation. We believe using these materials experimental realization of the one-hinge swimmer is possible. They have already demonstrated using these materials that they are able to recover the shape conformation for a one-armed swimmer and to extend it to a one-hinge swimmer should not be too challenging.

V. CONCLUSIONS

In this paper, we have modeled a two-dimensional scallop or a one-hinge swimmer. We have shown that the hydrodynamic interactions between the mass points of the swimmer and the fluid particles can be simulated using multi-particle collision dynamics (MPC). We have also demonstrated that if the arms of swimmer are very rigid, it follows the Scallop theorem and the swimmer is not able to propel itself through the viscous fluid. While when the arms are made flexible the time inversion symmetry is broken and swimmer performs ballistic motion. We have also shown that the velocity of the swimmer has a maximum, for intermediate bending rigidity along the arms of the swimmer. For small bending rigidity the arms are very flexible and the actuation is not able to produce the desired shape conformations, while for stiff arms we are closer to the Scallop theorem and the velocity goes towards zero. The reduced velocity is also studied as a function of frequency as well as the amplitude of actuation and we have shown a similar scaling relation as predicted by elastohydrodynamic within the small amplitude approximation even though we have considered large amplitude in the present work. We were also able to define Sperm number for the swimmer and also showed that the reduced velocity had a maximum at $S_p \sim 1.7$ consistent with what is expected for large amplitude actuation.

Acknowledgements

We would like to thank DST for funding and also would like to acknowledge IIT Delhi HPC facility for computational resources.

-
- [1] E. Lauga and T. R. Powers, *The hydrodynamics of swimming microorganisms*, Reports on Progress in Physics **72**, 096601, (2009).
 - [2] H. C. Berg and R. A. Anderson, *Bacteria Swim by Rotating their Flagellar Filaments*, Nature **245**, 380 (1973).
 - [3] H. C. Berg, *E. coli in Motion* (Springer, 2005).
 - [4] D. R. Mitchell, *Chlamydomonas flagella*, Journal of Phycology **36**, 261 (2000).
 - [5] B. T. M. Michael Oberholzer, Miguel A. Lopez and K. L. Hill, *Social motility in African trypanosomes*, PLoS Pathogens **6** (2010).
 - [6] S. B. Babu and H. Stark, *Modeling the locomotion of the African trypanosome using multi-particle collision dynamics*, New Journal of Physics **14**, 085012 (2012).
 - [7] D. Bray, *Cell movements: from molecules to motility* (Garland Science, 2001).
 - [8] J. Gray and G. Hancock, *The propulsion of sea-urchin spermatozoa*, Journal of Experimental Biology **32**, 802 (1955).
 - [9] A. Pacey, J. Cosson, and M. Bentley, *The acquisition of forward motility in the spermatozoa of the polychaete Arenicola marina*, Journal of experimental Biology **195**, 259 (1994).
 - [10] G. Taylor, *Analysis of the Swimming of Microscopic Organisms*, Proceedings of the Royal Society of London A: Mathematical, Physical and Engineering Sciences **209**, 447 (1951).
 - [11] E. M. Purcell, *Life at low Reynolds number*, American Journal of Physics **45**, 3 (1977).
 - [12] J. E. Avron and O. Raz, *A geometric theory of swimming: Purcell's swimmer and its symmetrized cousin*, New Journal of Physics **10**, 063016 (2008).
 - [13] A. Najafi and R. Golestanian, *Simple swimmer at low Reynolds number: Three linked spheres*, Phys. Rev. E **69**, 062901 (2004).
 - [14] E. M. Purcell, *The efficiency of propulsion by a rotating flagellum*, Proceedings of the National Academy of Sciences **94**, 11307 (1997).
 - [15] C. H. Wiggins and R. E. Goldstein, *Flexive and Propulsive Dynamics of Elastica at Low Reynolds Number*, Phys. Rev. Lett. **80**, 3879 (1998).
 - [16] M. C. Lagomarsino, F. Capuani, and C. Lowe, *A simulation study of the dynamics of a driven filament in an Aristotelian fluid*, Journal of Theoretical Biology **224**, 215 (2003).
 - [17] M. L. R. M. F. H. A. S. Remi Dreyfus, Jean Baudry and J. Bibette, *Microscopic artificial swimmers*, Nature **437**, 862 (2005).
 - [18] E. Lauga, *Floppy swimming: Viscous locomotion of actuated elastica*, Physical Review E **75**, 041916 (2007).
 - [19] S. Babu and H. Stark, *Dynamics of semi-flexible tethered sheets*, The European Physical Journal E: Soft Matter and Biological Physics **34**, 1 (2011).
 - [20] M. Allen and D. Tildesley, *Computer Simulation of Liquids* (Oxford: Clarendon Pr, 1987).
 - [21] G. Gompper, T. Ihle, D. M. Kroll, and R. G. Winkler, "Multi-particle collision dynamics: A particle-based mesoscale simulation approach to the hydrodynamics of complex fluids", in *Advanced Computer Simulation Approaches for Soft Matter Sciences III*, edited by C. Holm and K. Kremer (Springer Berlin Heidelberg, Berlin, Heidelberg, 2009) pp. 1-87.
 - [22] A. Malevanets and R. Kapral, *Mesosopic model for solvent dynamics*, The Journal of chemical Physics **110**, 8605 (1999).
 - [23] A. Malevanets and R. Kapral, *Solute molecular dynamics in a mesoscale solvent*, The Journal of Chemical Physics **112**, 7260 (2000).
 - [24] Y. Yang, J. Elgeti, and G. Gompper, *Cooperation of sperm in two dimensions: Synchronization, attraction, and aggregation through hydrodynamic interactions*, Phys. Rev. E **78**, 061903 (2008).
 - [25] Jinglei Hu, Mingcheng Yang, Gerhard Gompper, and Roland G Winkler, *Modelling the mechanics and hydrodynamics of swimming E. coli*, Soft matter, **11** (2015).
 - [26] Jan L Munch, Davod Alizadehrad, Sujin B Babu, and Holger Stark, *Taylor line swimming in microchannels and cubic lattices of obstacles*, Soft matter, **12** 2016.
 - [27] Mario Theers, Elmar Westphal, Gerhard Gompper, and Roland G Winkler, *Modeling a spheroidal microswimmer and cooperative swimming in a narrow slit*, Soft matter, **12**, 2016.
 - [28] M. T. Downton and H. Stark, *Simulation of a model microswimmer*, Journal of Physics: Condensed Matter **21**, 204101 (2009).
 - [29] A. Zottl and H. Stark, *Nonlinear dynamics of a microswimmer in Poiseuille flow*, Physical review letters **108**, 218104 (2012).
 - [30] C. H. Wiggins, D. Riveline, A. Ott, and R. E. Goldstein, *Trapping and wiggling: Elastohydrodynamics of driven microfilaments*, Biophysical Journal **74**, 1043 (1998).
 - [31] T. Ihle and D. M. Kroll, *Stochastic rotation dynamics: a Galilean-invariant mesoscopic model for fluid flow*, Physical Review E **63**, 020201 (2001).

- [32] T. Ihle and D. M. Kroll, *Stochastic rotation dynamics. I. Formalism, Galilean invariance, and Green-Kubo relations*, Physical Review E **67**, 066705 (2003).
- [33] J. T. Padding and A. A. Louis, *Hydrodynamic interactions and Brownian forces in colloidal suspensions: Coarse-graining over time and length scales*, Physical Review E **74**, 031402 (2006).
- [34] O. S. Pak and E. Lauga, *Fluid-Structure Interactions in Low-Reynolds-Number Flows* (Royal Society of Chemistry, 2015) pp. 100-167.
- [35] C. P. Lowe, *Dynamics of filaments: modelling the dynamics of driven microfilaments*, Philosophical Transactions of the Royal Society of London B: Biological Sciences **358**, 1543 (2003).
- [36] E. Gauger and H. Stark, *Numerical study of a microscopic artificial swimmer*, Phys. Rev. E **74**, 021907 (2006).
- [37] T. Qiu, T.C. Lee, A. G. Mark, K. I. Morozov, R. Munster, O. Mierka, S. Turek, A. M. Leshansky, and P. Fischer, *Swimming by reciprocal motion at low Reynolds number*, Nature communications **5** (2014).
- [38] N. Heddergott, T. Kruger, S. B. Babu, A. Wei, E. Stellamanns, S. Uppaluri, T. Pfohl, H. Stark, and M. Engstler, *Trypanosome motion represents an adaptation to the crowded environment of the vertebrate bloodstream*, PLoS Pathog **8**, e1003023 (2012).
- [39] C. Huang, J.a. Lv, X. Tian, Y.Wang, Y. Yu, and J. Liu, *Miniaturized swimming soft robot with complex movement actuated and controlled by remote light signals*, Scientific reports **5** (2015).
- [40] Y. Yu, M. Nakano, and T. Ikeda, *Photomechanics: directed bending of a polymer film by light*, Nature **425**, 145 (2003).